5

The formation and evolution of layered structures in porous media

Abstract

Horizontally layered structures can develop in porous or partially molten environments, such as magma chambers, hydrothermal systems and the early Earth's mantle. Since porosity is typically very low in these natural environments, double-advective instabilities may play a large role during the layer formation. By performing numerical experiments in which a rigid low-porosity medium is heated from below, we have studied the formation and evolution of layers in the initially stably stratified interstitial liquid. Growth of a convective layer through convective entrainment, the formation of a stable density interface on top of the layer and destabilization of the next layer are intimately linked. By monitoring the heat (solute) fluxes, it is observed that the transport of heat (solute) across the interface changes from convective entrainment toward a regime in which transfer is purely diffusive (dispersive). Since this transition occurs before the stage at which the lower layer arrives at the thermal equilibrium, we conclude that the transition in the entrainment regime limits the layer growth: the layer growth stops when the density interface on top has grown sufficiently strong to keep the ascending plumes in the lower layer from convectively entraining more fluid from above. A simple balance between the most important forces, exerted on a fluid parcel in the lower convective layer, is proposed as to determine this transition. The proposed force balance also indicates whether a density interface stays intact, migrates upwards or breaks down during the subsequent evolution of the layered sequence. Mechanical dispersion tends to increase transport of chemically dissolved elements across the density interface. Since this reduces the density difference between the two adjacent layers, the layer thickness increases. The results are discussed with respect to the geophysical scenarios mentioned above.

5.1 Introduction

Layering is a characteristic geological feature, on nearly every scale. These horizontally layered structures can develop in porous or partially molten systems such as magmatic intrusions [*Cawthorn,* 1996], the early Earth's mantle [*Stevenson,* 1989; *Olson et al.,* 1990], or

In revision by Schoofs, Trompert and Hansen for *Phys. Earth Planet. Int., 1999.*

hydrothermal systems [*Bischoff and Rosenbauer*, 1989; *Fournier*, 1990; *Williams*, 1997; *Oldenburg and Pruess*, 1998]. We are interested in the generation and evolution of convective layers within the fluid, which percolates through the pores and fractures of solid rocks.

In Chapter 4, double-diffusive convection (DDC) was shown to be a good potential candidate to generate layered structures in porous or partially molten environments. In order to reveal to fundamental features of the layer formation, the porosity was chosen equal to a hypothetical value of $\phi^* = 1$. However, in this so-called Hele-Shaw approximation heat and solute advect at the same speed. This approximation differs from flow in natural porous media in which porosity is typically low (see also Chapter 2). Diffusion of heat within the solid rock therefore results in the retardation of heat as compared to solute during advection, a process which gives rise to double-advective instabilities.

In this chapter, the results of a set of numerical experiments in the more realistic setting of a low-porosity medium are described. Despite the significant numerical challenge we have decided to do so in order to be able to investigate the potential role of DDC as a layer-forming mechanism in a natural porous medium. Comparing the results with those, as obtained in Hele-Shaw cells, enables us to delineate specific features of double-diffusive, double-advective flow as present in convection in low-porosity environments.

Beyond the interest in the evolution of geological systems the experiments will shed some light on fundamental differences in the flow dynamics of convection in porous media and in purely viscous flow (in the following free flow, in contrast to flow in porous media). Since inertial forces do not exist in porous media flow, significant differences are to be expected. For example, entrainment of non-buoyant fluid from a density gradient into a convective region is reduced by the absence of inertial forces. Further, drag forces exerted by the solid rock dominate over viscous coupling. Due to the lack of advection or diffusion of vorticity in porous media flow, the flow geometry is different from that of free flow. Moreover, viscous dissipation of energy is proportional to the square of velocity, but does not depend on the actual flow geometry [*Shen and Veronis*, 1991]. Energy dissipation in free flow, on the other hand, is mainly caused by viscous coupling between the fluid parcels [*Batchelor*, 1968]. Viscous coupling involves the spatial derivatives of velocity and, therefore, it is related to the scale of convection. Understanding these fluid dynamical phenomena is of vital interest towards a better understanding of the dynamics of the envisaged geological systems.

The model configuration is similar to the one used in the previous chapter (see Figure 4.1): a rectangular domain of aspect ratio $A = 0.5$ with impermeable boundaries. In a first set of experiments, the system of equations describing the flow is composed also of the same equations as before: (2.16) - (2.18). A thermal contrast is imposed at the bottom, while the temperature at the top is fixed to zero. The vertical walls are insulators with respect to heat transport, while all sides satisfy no-flux conditions for the solute. Initially, the motionless interior is cold and the solute concentration is stably stratified, having a linear gradient $\partial\hat{C}/\partial\hat{z} = 1$.

In addition to advective and diffusive transport of chemical elements, hydrodynamic mixing of the interstitial fluid at the pore scale also leads to chemical transfer. This type of mixing, called mechanical dispersion, is due to obstructions and the fact that all pores may not be accessible to a fluid element after it has entered a particular flow path [*Nield and Bejan*, 1992]. A further set of experiments addresses the mechanical dispersion explicitly, by replacing equation (2.18) with equation (2.19). Due to substantial heat diffusion through the solid rocks, mechanical dispersion of heat is negligible under most geological circumstances.

The outline of this chapter is as follows. The results of two sets of experiments with first, a scalar and, next, a velocity-dependent dispersion model are discussed in section 5.2. The chapter ends with a summary of the results and a discussion of its implications to the

geophysical settings mentioned above.

5.2 Results and discussion

The main objective of this study is to understand the formation and evolution of vertically stacked convective layers in low-porosity systems. Therefore a number of calculations has been carried out with various values of Ra_T, R_ρ, ϕ^*, and a_l, in a domain with aspect ratio $A = 0.5$. The numerical discretization used is 128×256 cells based on extensive testing by using various grids and varying the time step size.

First, the observations on the generation of convective layers in a typical low-porosity experiment are described. The parameters are $Ra_T = 5 \times 10^4$, $R_\rho = 4$, and $\phi^* = 0.1$. An effective chemical dispersion coefficient is taken, which is 100 times lower than the thermal diffusivity ($Le_{\text{eff}} = 100$). Next, the results of this experiment are compared with those observed in a Hele-Shaw cell in which $\phi^* = 1$. In section 5.2.2, the data are analyzed in order to understand what limits the height of the growing convective layers. The variety of the layer scales is discussed in terms of a balance between the most important forces acting on a fluid parcel in the lower layer (section 5.2.3). A sensitivity study of the layer generating mechanism as a function of the most important parameters is presented in section 5.2.4. In section 5.2.5, finally, the influence of mechanical dispersion on the layer formation is discussed.

5.2.1 Layer formation

In Figure 5.1, the thermal and compositional distributions are shown at four different stages in the evolution. A dark (light) shading indicates a high (low) temperature or enriched (depleted) compositional concentration. Figures 5.2a-5.2c display the corresponding vertical profiles of horizontally averaged temperature, composition and density. In Figure 5.2d, a set of different density profiles are displayed to provide an overview of the evolution of the layer formation.

Figure 5.1a and profiles i in Figure 5.2 display a thin thermal boundary layer developing at the bottom. Due to the large temperature difference across this layer, it becomes unstable almost instantaneously. Several convective plumes rise from this boundary layer into the cold and compositionally lighter environment. The region near the bottom is rapidly mixed by the rising and sinking currents, leading to a chemically almost uniform layer with increasing temperature. The ascending plumes erode the initial density gradient by incorporating the nonbuoyant fluid into the convective layer. This mechanism, which we call 'convective entrainment', increases the layer thickness with time.

Between the plume heads and the overlying fluid a sharp, stable density interface develops. The stability of the density jump arises from the difference in solute content between the convective layer and the motionless fluid above the interface. The vast majority of the plumes are stopped by this interface, while only the most vigorous ones are able to entrain further some material from the upper layer. While low solute flux across the interface keeps the interface intact, heat flux destabilizes the overlying fluid. As a result, a small convective layer develops on top of the lower one (see Figure 5.1b and profiles ii in Figure 5.2). This second layer also grows vertically by entraining fluid from above.

Convective mixing in the upper layer increases the chemical difference between the two layers, while the diffusive interfacial heat transfer reduces the temperature difference across the interface. Both processes lead to a further increase of the density difference $\Delta\hat{\rho}_{\text{int}}$ between both layers. As a result, fewer and fewer plumes can entrain material from above such leading to a further decrease in the growth rate. Figure 5.1c and profiles iii in Figure 5.2 show the

stage, in which the growth rate of the first layer is virtually zero. Advective mixing of the fluid in the second layer results in a chemically uniform layer with sharp boundary layers. The fluid on top of the second layer has also become unstable, which indicates that a third layer will soon be generated. All together, a staircase of well-mixed convective layers develops, which are separated by sharp diffusive/dispersive interfaces. Note that the lowermost layer is much thicker than the other ones.

Figure 5.1d and profiles iv in Figure 5.2 depict the situation at a later stage, in which the second and third layers have merged again and the amalgamized layer has just reached its maximal thickness. Note that another layer initiates on top of the amalgamized layer. When the heat which enters the domain through the bottom is sufficiently large to destabilize all fluid, the convective layers will reach the top of the domain and the interfaces start to break down one after each other from the top down (not shown). Ultimately, one chemically homogeneous convective layer remains.

Up to now, the gross features of the layer formation in a low-porosity medium resemble those observed in experiments in a Hele-Shaw cell (where $\phi^* = 1$). However, there exist also a number of significant differences in the evolution of the convective layers within these two media. In order to reveal these differences a simulation with $\phi^* = 1$ has been performed, while keeping the other parameters as before. Figure 5.3 depicts snapshots of the $\hat{T}$ and $\hat{C}$ fields and the horizontally averaged profiles of $\hat{T}$,$\hat{C}$ and $\hat{\rho}^*$, at the same stage as Figure 5.1b and the profiles ii in Figure 5.2. Two layers have developed in the lower part of the domain, while a third one just starts to destabilize. Furthermore, the density contrast across the interface between the first two layers is relatively small (the profile of $\hat{\rho}^*$ shows that $\Delta\hat{\rho}^*_{\mathrm{int}} \approx 5 \times 10^3$). Hence, the interface fluctuates considerably.

The most striking difference is that, at the stage shown, the first convective layer in the low-porosity experiment has already grown significantly larger ($\hat{h} = 0.52$), as compared with the first layer in the Hele-Shaw experiment ($\hat{h} = 0.21$). The average temperature of the first layer, on the other hand, is lower in the low-porosity medium. Due to the high advection rate of the solute in a low-porosity medium, virtually all available potential energy is converted into kinetic energy almost instantaneously. Therefore, heat which enters the domain through the bottom leads to advective homogenization of the compositional field (and thus to a fast layer growth), rather than to an increase of the internal energy of the convective layer (due to the upward advection of heat).

A consequence of the relatively fast layer growth in the low-porosity medium is that the density jump on top of the layer also grows at a faster rate, than is the case in the Hele-Shaw experiment (compare the density profiles). This phenomenon will turn out to be of significant importance for the self-limiting mechanism of the convective layers. Due to the fast growth of the density contrast between the convective layer and the motionless fluid, the interface is virtually flat almost from the point of destabilization of the convective layer.

Another specific feature of low-porosity flow is that vertical fluid exchange occurs on a smaller lateral scale than is the case in Hele-Shaw flow. As far as we know, it has not been clarified yet what exactly determines the cell width in porous media flow. Due to the lack of viscous coupling particular to flow in porous media [*Shen and Veronis*, 1991], this slender flow pattern does not inherently lead to an extreme loss of energy by viscous dissipation, as would be the case for free flow. The rapid exchange of chemically buoyant (depleted) and heavy (enriched) fluid is, at least locally, a very efficient mixing mechanism.

Finally, we note that the ascending plumes often detach from the bottom thermal boundary layer in the low-porosity experiments, rather than ascending straight to the top of the convective layer (as is the case in Hele-Shaw experiments). The ascending plume parts deflect or split up when encountering sinking currents.

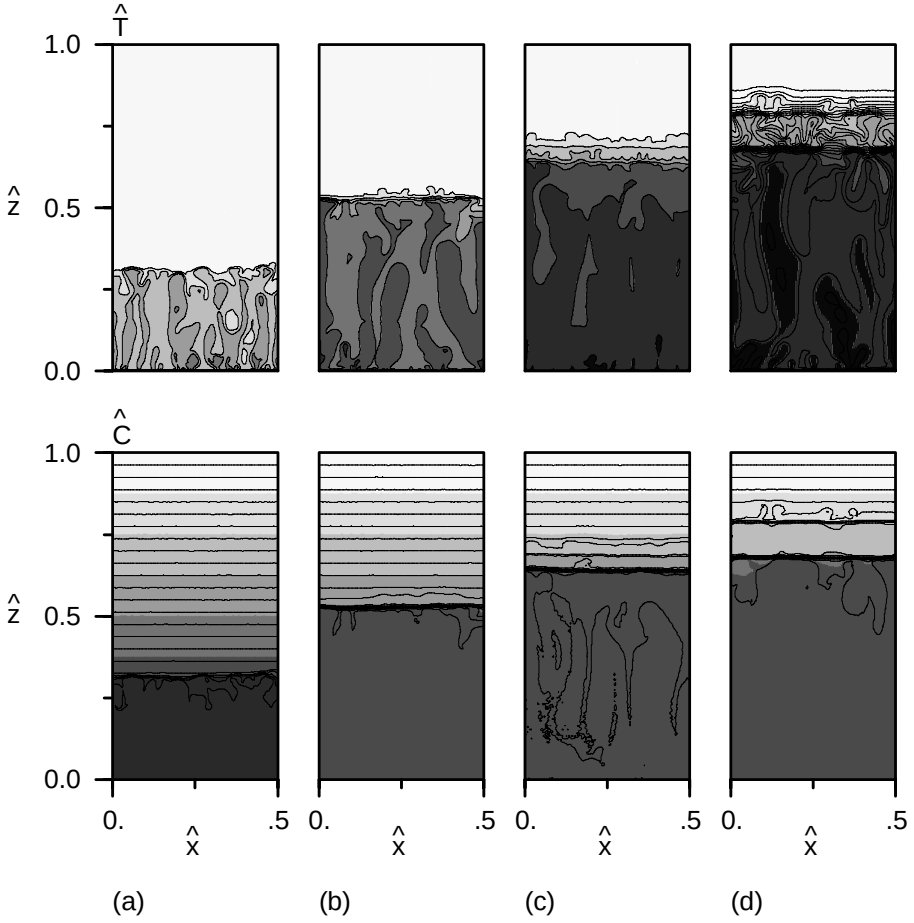

Figure 5.1: Snapshots of temperature $\hat{T}$ and compositional concentration $\hat{C}$ of a simulation with $Ra_T = 5 \times 10^4$, $R_\rho = 4$, $Le_{\text{eff}} = 100$, and $\phi^* = 0.1$ at (a) $\hat{t} = 0.000438$, (b) $\hat{t} = 0.002788$, (c) $\hat{t} = 0.004733$, and (d) $\hat{t} = 0.007951$. Dark (light) shading indicates high (low) temperature or enriched (depleted) compositional concentration. In the $\hat{C}$ snapshots and the $\hat{T}$ ones in Figures 2b-2d the contour interval is 0.05. Contours in the $\hat{T}$ snapshot in Figure 2a are spaced at an interval of 0.1, as to show more clearly the thermal evolution of the first layer.

5.2.2 Self-limitation of the convective layers

Of vital importance in understanding the layer formation is the question what limits the convective layer to a certain height. In Hele-Shaw experiments, two mechanisms become operative nearly at the same stage during the evolution of the first layer (Chapter 4). First, transport of heat and solute across the interface changes from convective entrainment toward pure diffusion/dispersion across the interface. In this mechanism, the density jump on top of the layer

has grown sufficiently large to prohibit the plumes from entraining fluid from above into the convective layer. Note that this mechanism determines the limitation of the layer growth in free flow [*Fernando,* 1987; *Molemaker and Dijkstra,* 1997].

The second mechanism limiting the layer growth in Hele-Shaw cells is, that the convective

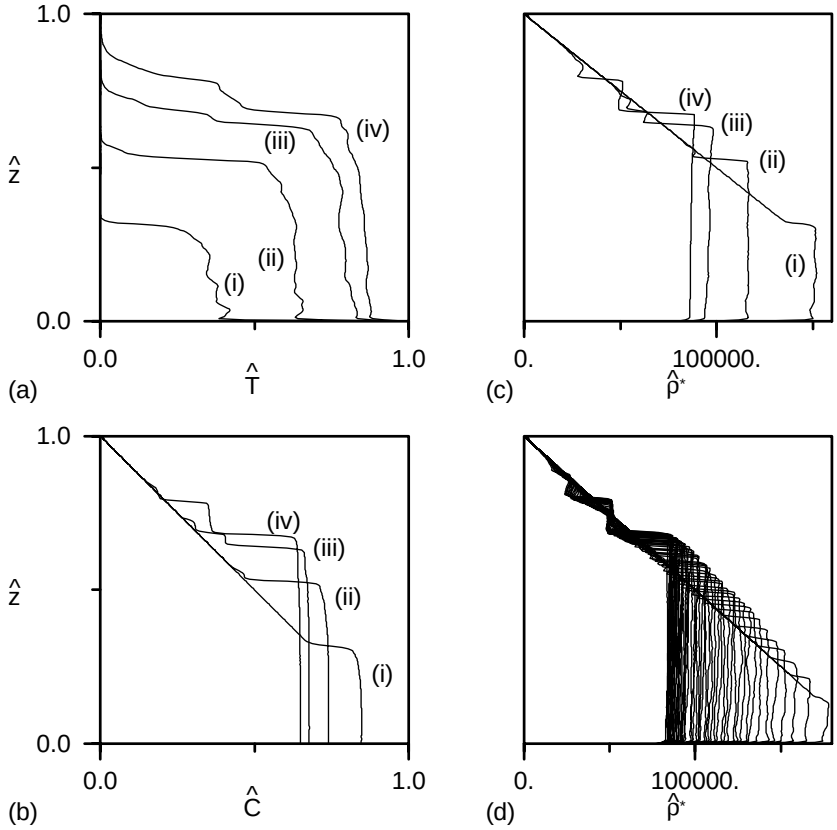

Figure 5.2: Transient development of horizontally averaged profiles at the same times as in Figure 5.1. (a) Temperature $\hat{T}$. (b) Compositional concentration $\hat{C}$. (c) Density $\hat{\rho}^* = \hat{\rho} - \hat{\rho}_0 = Ra_T(R_\rho \hat{C} - \hat{T})$. (d) Same as Figure 3c, but at many more times between $\hat{t} = 0.0$ and $\hat{t} = 0.01$. The development and sharpening of several interfaces is clearly shown.

layer reaches a thermal equilibrium. At this equilibrium, the heat flux through the horizontal boundary layers of the convective layer are equal, while the average temperature of the layer is constant. Consequently, the layer has stopped growing and the flow within resembles a statistically steady state. The flow does not really reach a statistically steady state, because diffusive (dispersive) interfacial heat (solute) transfer erodes the density jump across the interface on a compositionally dispersive time scale. This mechanism of arrival at a thermal equilibrium was actually proposed as to determine the limitation of the convective layers in Hele-Shaw cells (Chapter 4).

A third mechanism was proposed earlier for free flow and it implies that a stationary situation is reached when entrainment from below the interface by convection in the upper layer balances entrainment from above the interface by convection in the lower layer [*Turner,*

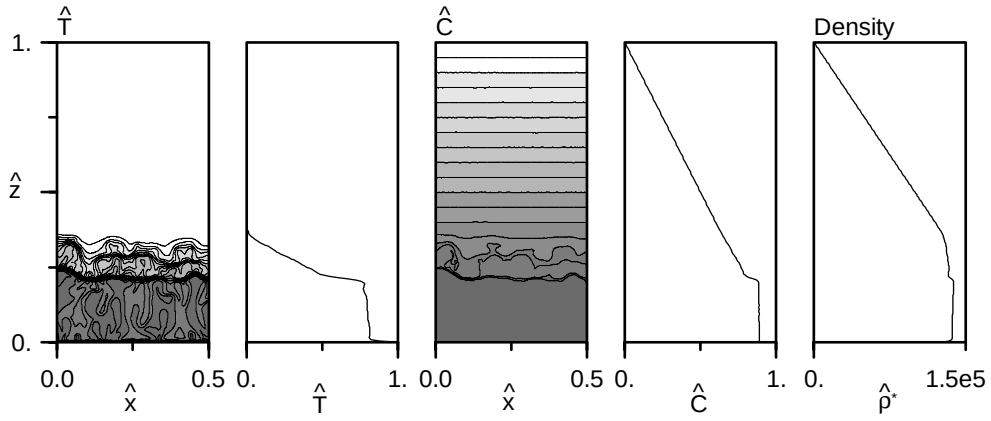

Figure 5.3: Snapshots of the $\hat{T}$ and $\hat{C}$ fields and the horizontally averaged profiles of $\hat{T}$,$\hat{C}$ and $\hat{\rho}^*$ of a Hele-Shaw experiment, plotted at the same stage as the snapshots (b) and profiles (ii) of the previous figures. Parameters are $Ra_T = 5.10^4$, $R_\rho = 4$, $Le_{\text{eff}} = 100$, and $\phi^* = 1$. The contours are uniformly spaced at an interval of 0.05.

1968; *Huppert and Linden*, 1979]. Though this mechanism has been shown to be unimportant for the Hele-Shaw case (Chapter 4), it might be a possible cause of the layer limitation in low-porosity flow.

In order to investigate if and which one of these mechanisms is relevant in low-porosity media, we have focused our attention on the evolution of the first convective layer. The different stages can be summarized as follows (Figure 5.4): in the first phase the layer grows very fast by entraining fluid from above the interface (from the start up to arrow 2). Meanwhile, a density jump develops on top of the convective layer. This is followed by a period of decreased growth rate (stage confined between arrows 2 and 3). During this phase, the density difference across the interface on top of the first layer grows further gradually. Moreover, the fluid above the interface becomes unstable such leading to the formation of the second layer. After this intermediate stage, finally, another sharp decrease in the growth rate is observed (arrow 3). From this point, the thickness of the first layer increases only very slowly up to the end of the simulation. Arrow 4 corresponds with the stage at which the second layer stops growing. This is discussed in section 5.2.3.

In order to distinguish between the three mechanisms, we have monitored the transport properties near the interface. For the balanced entrainment mechanism to be relevant, one expects a significant advective component of heat and mass flux across the interface. The two other mechanisms, on the contrary, are characterized by a transition from convective toward purely diffusive/dispersive interfacial transport. The horizontally averaged diffusive/dispersive fluxes of heat and solute are defined by equations (4.1) and (4.2).

The results of the measurements are shown in Figure 5.5. Horizontally averaged fluxes are plotted at four time instants, corresponding to those marked in Figure 5.4 (the dashed profiles of the fourth instant and will be discussed in section 5.2.3). Each profile has been time averaged over a number of profiles around these time instants. As expected, in the well-mixed convecting layer the advective fluxes are much larger than the diffusive ones. Moreover, the magnitude of the compositional advective flux is much larger than that of heat again, due to both a high Le_{eff} and a low porosity.

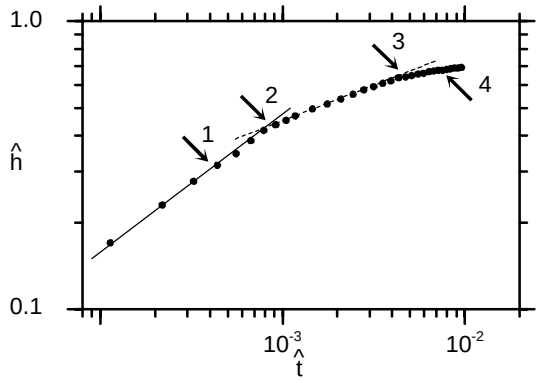

Figure 5.4: Temporal evolution of the height h of the first layer of the low-porosity experiment depicted in Figures 2 and 3. The numbered arrows indicate the times of the snapshots and profiles depicted in the previous figures.

At the first time instant (solid curves), the advective components of both heat and solute fluxes dominate the transport on top of the convective layer. This indicates that fluid is advectively entrained from above into the first layer. The sharp peaks in the diffusive profiles demonstrate the flatness of the interface (at $\hat{z} = 0.31$, indicated by arrow 1).

At the second time instant (dotted curves), the advective component of the heat flux across the interface is approximately zero, while the advective solute flux still dominates the dispersive one. Entrainment across the interface has decreased, because the density difference between the two convective layers has increased. Nevertheless, fluid from the second layer is entrained slowly into the lowermost one.

Finally, the dash-dotted curves show the fluxes shortly after the second change in the growth rate. The position of the interface is at $\hat{z} = 0.64$, denoted by arrow 3. At this stage, both heat and solute fluxes across the interface are diffusively/dispersively dominated.

The flux measurements across the interface thus reveal a transition from a regime in which convective entrainment dominates, toward a regime in which the transport is purely diffusive/dispersive. These findings therefore rule out the mechanism of balanced entrainment and seem to indicate that either the transition in the entrainment regime itself, or the arrival at a thermal equilibrium, limits the convective layers. It is remarkable to say that these observations resemble closely the observations in Hele-Shaw cells.

One way to distinguish between these two remaining mechanisms is by comparing the incoming and outgoing fluxes of the driving component (heat) of the layer. For the first mechanism to be valid, the heat flux through the interface is still smaller than the bottom heat flux, at the stage when the layer growth stops. In the second mechanism, these two fluxes have become equal at that stage.

The heat fluxes through both boundary layers of the first convective layer are compared at the same three time instants as before. Heat flux through the bottom of this layer is always purely diffusive, because the bottom of the domain is impermeable. At the position just above the bottom boundary layer, the advective heat flux is nearly equal to the bottom heat flux. At the first time instant, the bottom heat flux is equal to 142 dimensionless units which is much larger than the total heat flux through the sharp density interface. During the stage of decreased growth rate, the bottom heat flux is approximately 74 dimensionless units, three times larger as compared to the interfacial heat flux. At the moment when the layer growth

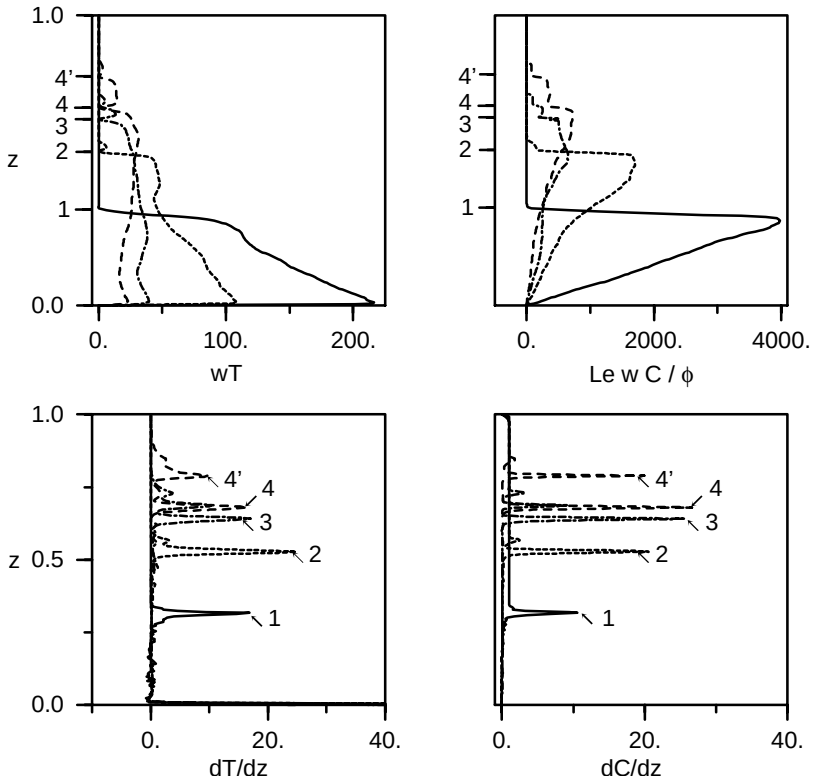

Figure 5.5: Horizontally averaged diffusive/dispersive and advective fluxes of $\hat{T}$ and $\hat{C}$, as defined in (4.1) and (4.2), plotted as a function of depth, at the same four stages in the evolution as in Figure 5.1: $\hat{t} = 0.000438$ (solid curves, 1), $\hat{t} = 0.002788$ (dotted, 2), $\hat{t} = 0.004733$ (dash-dotted, 3), and $\hat{t} = 0.007951$ (dashed, 4). The numbered arrows indicate the position of the first interface in the diffusive/dispersive profiles at the four stages. The arrow with 4' indicates the second interface at the fourth stage.

stops, the bottom heat flux is approximately 41, still more than twice as large as compared to the heat flux across the interface (which is equal to 17).

From these measurements, we can conclude that the layer growth stops before the first layer arrives at the thermal equilibrium. We therefore favor the transition in the entrainment regime, as to determine the final thickness of this layer in low-porosity systems. When the density jump on top of the layer becomes sufficiently strong to prohibit the plumes to entrain fluid from above, heat (solute) transfer across this interface becomes purely diffusive (dispersive). Note that this mechanism is different from the one which limits the layer growth in Hele-Shaw cells (Chapter 4). Despite the lack of inertial and viscous forces, on the other hand, the limiting mechanism in porous media flow is similar as that in free flow [*Molemaker and Dijkstra*, 1997]. Further heating of the layer leads to only minimal additional growth until the thermal equilibrium is reached.

The next question we want to answer is, what determines the transition in heat and solute transport across the interface. In free flow, this transition in the entrainment regime is described by a balance between the kinetic energy of the lower convective layer and the

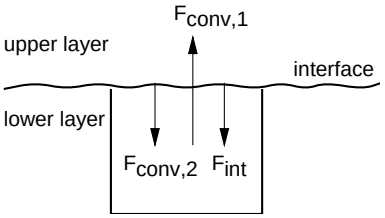

Figure 5.6: Schematic diagram of two convective layers separated by a density interface. A fluid parcel just beneath the interface experiences two forces: a convective force of the lower layer $\mathbf{F}_{\mathrm{conv},1}$, and a buoyancy force due to the density difference across the interface $\mathbf{F}_{\mathrm{int}}$.

potential energy across the interface [*Fernando*, 1987; *Molemaker and Dijkstra*, 1997].

At a first glance, a similar balance could also determine the transition in transport mechanism in porous media flow. For the buoyancy-driven convection of a fluid in a porous material, however, inertia is negligible (see section 5.2.2). In other words, the flow reacts instantaneously on the buoyancy and pressure gradients present in the fluid. Rather than an energy balance, a balance between the buoyancy forces acting on the fluid just beneath the interface seems therefore to be more appropriate to describe the transition in low-porosity flow.

In Figure 5.6, a schematic diagram is shown of the convecting bottom layer, the density interface and the convecting layer on top of the interface. A fluid parcel just beneath the interface experiences the following forces. First, the upward convective force $\mathbf{F}_{\mathrm{conv},1}$ is given by the buoyancy of the parcel minus the pressure gradient, divided by ϕ^*:

$$\mathbf{F}_{\mathrm{conv},1} = \frac{\overline{\hat{\rho}^* - \partial\hat{p}/\partial\hat{z}}}{\phi^*} = \frac{\hat{w}}{\phi^*}, \tag{5.1}$$

where Darcy's law has been used. Subscript 1 denotes that it is the convective force, which is present in the first layer. The factor ϕ^* is included because the solute advects upwards with a speed of $\hat{w}/\phi^*$, rather than $\hat{w}$. Obviously, the vertical velocity becomes negligible at the interface, which would give a convective force $\mathbf{F}_{\mathrm{conv},1}$ equal to zero. This can be seen in Figure 5.7a, in which the vertical profiles of both the horizontally averaged and maximum vertical velocity are plotted, just at the stage at which the layer growth stops. As an alternative, a representative value of the upward velocity in the lower layer can be taken as to represent the convective force. Since only the most vigorous plumes are able to scrape off the interface, we choose the maximal vertical velocity $\hat{w}_{\max}$ in the lower convective layer, divided by ϕ^*, as the convective force $\mathbf{F}_{\mathrm{conv},1}$.

The second force, which acts on the fluid parcel, is exerted by the stable density interface and is directed downwards. Its dimensionless, absolute value is given by $|\mathbf{F}_{\mathrm{int}}| = |\overline{\Delta\hat{\rho}^*_{\mathrm{int}}}|$, which is the horizontally averaged density difference across the interface. A third force, the downward convective force $\mathbf{F}_{\mathrm{conv},2}$ in the upper layer is neglected here, because it is still small at the moment when the layer growth stops.

We suggest that the transition in the entrainment regime occurs when:

$$\mathbf{F}_{\mathrm{conv},1} = c_1\,|\mathbf{F}_{\mathrm{int}}|, \tag{5.2}$$

where c_1 should be of order $O(1)$. In order to check this force balance, we have plotted both forces as a function of time (Figure 5.7b). The downward interfacial force $|\mathbf{F}_{\mathrm{int}}|$ initially increases strongly with time toward a value of 2.70×10^4 at $\hat{t} \approx 0.0001$. From this point, $|\mathbf{F}_{\mathrm{int}}|$ grows at a significantly lower rate. The convective force $\mathbf{F}_{\mathrm{conv},1}$, on the other hand,

first decreases strongly. At a later stage, the force decreases further gradually until an almost statistically steady value is reached. At the moment when the layer growth stops ($\hat{t} \approx 0.0045$), $\mathbf{F}_{\text{conv},1} \approx 3.60 \times 10^4$ and $|\mathbf{F}_{\text{int}}| \approx 3.92 \times 10^4$, which means that a constant c_1 of order $O(1)$ is obtained. This is a clear indication for the proposed force balance to be appropriate.

5.2.3 Variation in layer thicknesses

A typical feature of the layer formation is that the first convective layer is much thicker than all of the others which are fairly similar in scale (see Figure 5.1c-d). This might indicate that the final height of these next layers is determined by another mechanism, than is the case for the first layer.

In order to gain insight in the evolution of these other layers, we have examined the evolution of the amalgamized second layer. From the fluxes (Figure 5.5, dashed curves), we have observed a transition from convective entrainment toward pure diffusion (dispersion) of heat (solute) across the interface on top of this layer (indicated by arrow 4'). Moreover, the growth of this layer is limited before a thermal equilibrium has been reached. This can be seen in Figure 5.5 by comparing the diffusive heat fluxes near arrows 4 and 4' (as the advective heat fluxes are equal to zero across these interfaces). Since the mechanism, which limits this second layer, is similar to the mechanism which determines the layer height of the first layer, something else must be responsible for the difference in layer scales.

In our view, the temporal evolution of the vertical velocity, and thus the convective force, explains why the first layer is so much larger than all of the others (see Figure 5.7b). Just after destabilization of the bottom thermal boundary layer, the thermal contrast between the rising plumes and the still cold interior is huge. Consequently, the vertical velocities of these plumes, and thus the convective forces, are also very large. The increase of the temperature in the convective layer with time leads to a gradual decrease of the plume velocities, until from $\hat{t} \approx 0.005$ the maximal velocity is statistically constant. The interfacial density force, on the other hand, increases almost linearly with the thickness of the convective layer, but does not depend on the particular stage of the evolution. The force balance for the second layer is therefore reached already at a lower layer depth, as compared with the one for the first layer.

The gradual decrease of velocity in time toward a statistically constant value thus explains both the relatively larger thickness of the first layer and the almost equal vertical scales of the subsequent layers.

Two dynamical mechanisms have been observed, which influence the structure on a time scale much shorter than the dispersive one. These are gradual 'upward migration' and sudden 'breakdown' of the interface. Both phenomena are described in detail for the Hele-Shaw experiments in the previous chapter. These phenomena become better understandable in the frame of the proposed force balance.

For upward migration of an interface to occur, two conditions must be met. First, the convective force in the lower layer must be stronger than in the upper one. Secondly, the interfacial density force must be equal or smaller than the convective force in the lower layer. The rising plumes in the lower layer can then entrain fluid across the interface.

The breakdown of an interface occurs, on the other hand, when the magnitude of the convective forces in the two layers adjacent to the interface are (1) equal to each other and (2) of the same order as the density force. In this setting, the convection currents in both layers deflect the interface. When the amplitude of the deflections become so large, that the interface touches the interface above, the interface breaks down.

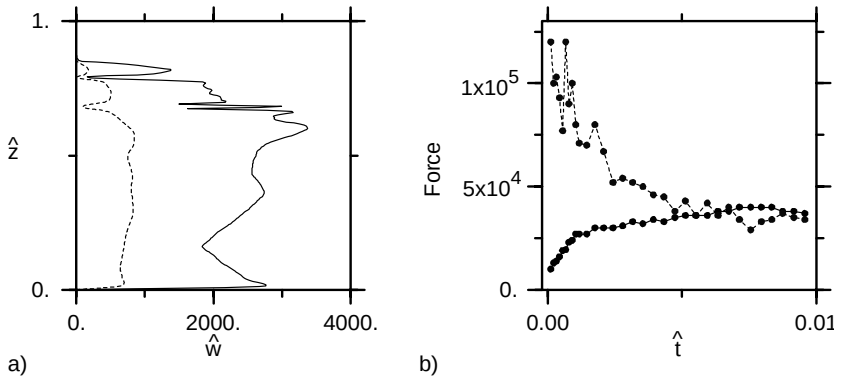

Figure 5.7: (a) Vertical profiles of the lateral maximum of the vertical velocity $\hat{w}_{max}$ (solid curves), and of the horizontally averaged vertical velocity (dotted), at the moment when the layer growth stops ($t = 0.004733$) . (b) The two forces depicted in (a), $\mathbf{F}_{\text{conv},1}$ (dotted) and $|\mathbf{F}_{\text{int}}|$ (solid), plotted as a function of time.

5.2.4 Parameter dependence

In this section, the sensitivity of behavior of the layer-forming mechanism to the most important parameters is described. In the first set of experiments the thermal Rayleigh number has been varied, while the other parameters are fixed to $R_\rho = 3$ and $\phi^* = 0.1$. For Rayleigh numbers up to $Ra_T < 15 \times 10^3$, the heat flux through the bottom is not large enough to destabilize more than one layer. At larger Ra_T, several layers are generated in the way as described in section 3.1, where the number of layers that form increases with increasing Ra_T. Figure 5.8a shows the final thickness of the first layer $\hat{h}_f$ as a function of Ra_T, for five simulations in this multiple layer regime. The results indicate that a power law relation exists between $\hat{h}_f$ and Ra_T, with an exponent of 0.2.

Since a higher Ra_T leads to a higher vertical velocity in the lowermost layer and thus to a larger convective force, this exponent seems unexpectedly low. From the experiments, we suggest the following relation between Ra_T and the maximum vertical velocity $\hat{w}_{\max}$:

$$\hat{w}_{\max} \propto Ra_T^{1.0}. \tag{5.3}$$

Therefore, the low sensitivity of the layer thickness on Ra_T must imply that besides the vertical velocity, the density difference across the interface also increases strongly with increasing Ra_T. This is understandable, because R_ρ is kept constant. Apparently, the forces associated with these two quantities increase at an almost similar rate.

Next, four experiments have been performed in which R_ρ is varied, while $Ra_T = 5 \times 10^4$ and $\phi^* = 0.1$. Figure 5.8b shows the resulting inverse relationship between the final layer thickness $\hat{h}_f$ and the buoyancy ratio R_ρ:

$$\hat{h}_f = 0.9\, R_\rho^{-1.4}. \tag{5.4}$$

Assumed that convection has been well developed in a layer, the interior of the layer is compositionally uniform. This means that the chemical field only influences the boundary layers. Consequently, the vertical velocity and thus the convective force of the first layer is merely a function of Ra_T (see equation (5.3)), and depends only weakly on the buoyancy ratio R_ρ. A

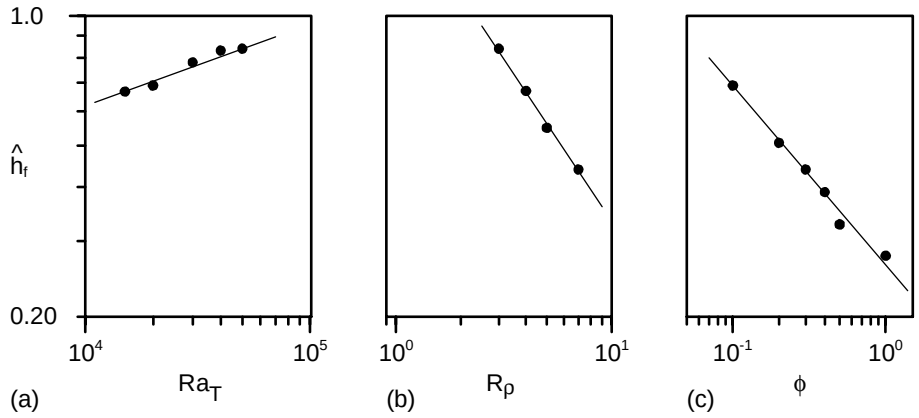

Figure 5.8: Sensitivity of behavior of the layer formation as a function of the most important parameters. (a) The final layer height of the first layer $\hat{h}_f$ as a function of Ra_T for a constant buoyancy ratio $R_\rho = 3$ and $\phi^* = 0.1$. (b) The final layer height $\hat{h}_f$, but now as a function of R_ρ, while the Rayleigh number is fixed to $Ra_T = 5.10^4$, and porosity is kept at $\phi^* = 0.1$. (c) The final thickness of the first layer $\hat{h}_f$, but now as a function of ϕ^*, while $Ra_T = 5 \times 10^4$ and $R_\rho = 3$.

higher chemical buoyancy does, however, enhance the growth of the density contrast across the interface such explaining the large negative exponent in (5.4).

In a further set of experiments porosity is varied, motivated by the fact that porosity is typically very low in magmatic and hydrothermal systems ($\phi^* \approx O(10^{-4} - 10^{-1})$). Flow at the very low porosities cannot be resolved numerically in this study. In order to find the relation between porosity and the final layer thickness $\hat{h}_f$, we have performed six simulations in which porosity ranges from 1 to 0.1 (Figure 5.8c). The other parameters are fixed at $Ra_T = 2 \times 10^4$, $R_\rho = 3$ and $Le_{\text{eff}} = 100$. A simple power law, that describes the data, is

$$\hat{h}_f = 0.28\, {\phi^*}^{-0.4}. \tag{5.5}$$

This relationship shows, that porosity does not only influence the convective force $\mathbf{F}_{\text{conv},1}$ within the lower layer (since in that case $\hat{h}_f \propto {\phi^*}^1$, see (5.1)), but also leads to a faster growth of the interfacial density force $|\mathbf{F}_{\text{int}}|$.

5.2.5 Mechanical dispersion

In the previous experiments, we have assumed an effective chemical dispersion coefficient, which is 100 times lower than the effective thermal diffusivity of the saturated medium. For the large velocities observed during the layer formation, however, mechanical dispersion may play a significant role in the transport of chemical elements. Laboratory experiments [*Griffiths,* 1981] showed that mechanical dispersion indeed modifies significantly the chemical flux across a horizontal density interface between two convecting layers. The scalar model (2.18) employed in the previous experiments is not very accurate in handling mechanical dispersion of chemical elements and is replaced by a more advanced tensor model (2.19) [*Bear,* 1972].

At present, both the longitudinal dispersivity a_l and the dispersivity ratio a_r, which appear in (2.19), are poorly known in geological media [*Gelhar et al.,* 1992]. In crustal domains of

less than a hundred meters, laboratory, bore hole and field tests seem to indicate that the longitudinal dispersivity is related to the scale of the flow domain systematically. However, the longitudinal dispersivity flattens to a value of around 1 to 10 meters for a domain scale of around 100 meters, suggesting that this so-called 'scale-effect' does not proceed to regional scales. The transversal dispersivity follows this behavior, but at values which are smaller by an order of magnitude. In partially molten magmatic systems, these hydraulic parameters are also not known very well. The layer-forming mechanism studied here may be applicable to either of these geological systems, which differ both in length scale and structure of the solid framework. The amount of mechanical dispersion may therefore vary significantly among these systems. Therefore, a sensitivity study of the layer formation to dispersion of chemical elements is necessary.

We have performed six experiments, in which the longitudinal dispersivity has been varied between two extreme values ($\hat{a}_l = 10^{-2}$ and 10^{-5}) while the dispersivity ratio is kept at $a_r = 10$. Molecular diffusivity of the chemical component is taken 10^4 times smaller than the effective thermal diffusivity ($Le_{\mathrm{mol}} = 10^4$). Other parameters are $Ra_T = 10^5$, $R_\rho = 3$, and $\phi^* = 0.5$.

Figure 5.9 depicts snapshots of the temperature and chemical fields of two experiments, at the same stage in the evolution. For a case in which the dispersivity is low ($\hat{a}_l = 10^{-5}$, Figure 5.9a), the final thickness of the first convective layer has just been reached. The observed layer height is nearly similar to that of the lowermost layer generated in the simple scalar dispersion experiment (in which $\hat{h}_f = 0.48$, see Figure 5.8c). Furthermore, several layers have developed on top of each other in a manner, which resembles the mechanism observed in the experiments with a simple scalar dispersion model fairly well.

In a system in which the longitudinal dispersivity is equal to 10^{-3} times the depth of the system, on the other hand, the dimensionless height of the first layer is already significantly larger at the same stage in the evolution (Figure 5.9b). Longitudinal dispersion of chemical elements in the ascending plumes and in less extent also transversal dispersion in currents along the interface mix the chemical content of the first layer with that of the fluid above the interface. Since these processes reduce the density difference across the interface, the plumes in the lower layer can entrain more fluid from above. This results both in a faster growth rate and a larger final thickness of the first layer, as compared with the low-dispersion experiment shown in Figure 5.9a. Finally, an even larger longitudinal dispersivity ($\hat{a}_l = 10^{-2}$) enables the first layer to grow to the top of the domain and prevents the generation of another layer. In Figure 5.10a, the final thickness of the first layer $\hat{h}_f$ is plotted for the six experiments as a function of $\hat{a}_l$.

Mechanical dispersion of chemical elements clearly increases the amount of entrainment across the interface. Therefore, it must be taken into account in the force balance (5.2) which determines the transition in the entrainment regime. Since the convective layer for $\hat{a}_l = 10^{-2}$ is limited by the vertical extent of the domain, this data point has not been taken into consideration here. Figure 5.10b depicts the value which the constant c_1 in (5.2) should take in order to match the two forces at the moment when the layer growth stops, as a function of $\hat{a}_l$. When we assume that transversal dispersion is negligible, a more complete force balance of the form

$$\mathbf{F}_{\mathrm{conv},1} = 10^{-5}\hat{a}_l^{-0.7}\,|\mathbf{F}_{\mathrm{int}}|. \tag{5.6}$$

is derived.

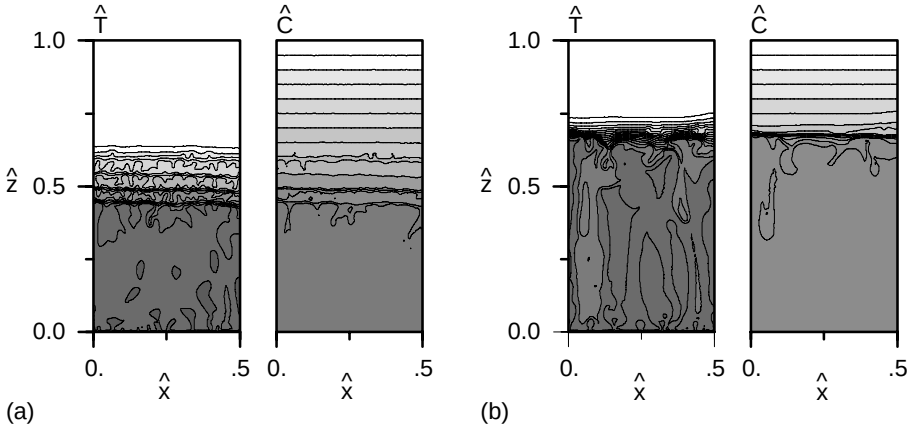

Figure 5.9: Snapshots of temperature and compositional concentration of two experiments at a similar stage during the evolution ($\hat{t} = 0.0046$). The longitudinal dispersivity is (a) $\hat{a}_l = 10^{-5}$ and (b) $\hat{a}_l = 10^{-3}$. Other parameters are: $Ra_T = 10^5$, $R_\rho = 3$, $\phi^* = 0.5$, $Le_{\mathrm{mol}} = 10^4$, and $a_r = 10$. The contours are uniformly spaced at intervals of 0.05.

5.3 Summary

The formation and evolution of horizontally layered structures in a low-porosity rigid medium has been studied, by imposing a temperature contrast at the bottom of a compositionally stably stratified fluid. In a first set of numerical experiments, chemical dispersion is represented by a simple effective scalar model. The results from these experiments show that thermochemical convection in a low-porosity medium is a vital mechanism for the generation of layered structures.

The gross features of the layer formation resemble those observed in Hele-Shaw cells. A convective layer develops at the bottom of the domain, which grows by incorporating fluid from above. Since this layer is convectively mixed, a stable density jump develops on top of the layer. The fluid overlying this density interface is destabilized by considerable heat flux across the interface, while low solute flux keeps the interface intact. In this way a staircase of well-mixed convective layers develops, of which the lowermost layer is much thicker than all of the others. The layers are separated by sharp diffusive/dispersive interfaces.

We have shown that the limitation of the first layer to a certain depth is not a consequence of destabilization of the next layer, as was proposed earlier for free flow [*Turner*, 1968]. In our configuration, the layer growth is limited by the formation of a sufficiently strong density interface on top of the layer. Consequently, the transport of heat (solute) across the interface changes from convective entrainment toward pure diffusion (dispersion). In that sense our results differ from those on flow in Hele-Shaw cells, where the layer growth is limited due to the arrival at the thermal equilibrium (Chapter 4).

We attribute the difference in the limiting mechanisms to fundamental differences in the dynamical behavior of the flow in these two media. In low-porosity media heat advects slower than solute by the factor of porosity, while in Hele-Shaw cells both quantities advect with the same velocity. As a result, thermal energy which enters the low-porosity domain through the bottom is converted into kinetic energy, rather than increasing the internal energy of the convective layer. Advective homogenization of the chemical field results in a relatively fast

growth of the density interface on the top of the layer. Consequently, the transition in the entrainment regime has occurred before the layer arrives at the thermal equilibrium. Note that despite the lack of inertia and viscous coupling, the limiting mechanism is similar to the one observed in free flow [*Fernando,* 1987; *Molemaker and Dijkstra,* 1997].

A simple force balance on a fluid parcel in the lower layer is proposed as to determine the limitation of the layer growth. The layer growth stops when the upward convective force of the lower layer becomes smaller than the downward directed force exerted by the stable density difference across the interface. The depth of the layer is determined by the amount of fluid which can be entrained within the period before the transition in the entrainment regime has occurred.

The variation of layer thickness between the first and other layers is ascribed to a decay of the convective forces in time, toward a statistically steady value. Since these other layers develop at a later stage in the evolution of the system, the convective forces in these layers are lower as compared to the force which enabled the first layer to grow. As a result, the transition in the entrainment regime takes already place at a lower layer height.

Once it is established, an interface can vanish through three mechanisms. Besides (1) the ultimate disappearance of any interface through diffusional/dispersive homogenization, our experiments have shown that on short time scales (2) the migration of an interface and (3) the breakdown of an interface can lead to sudden changes of the layer structure. These intermittent changes determine the vertical scales of the convective layers, rather than the initial layer growth. The different behavior of the two dynamical vanishing mechanisms is interpreted in terms of the balance between the most important forces.

From this set of experiments, we have the following indications with respect to parameter dependence. First, the number of layers that develops is determined by the thermal Rayleigh number, while it is not very sensitive to the buoyancy ratio. Note that relatively high thermal Rayleigh numbers are necessary to develop multiple layers, which means that a high temperature contrast and/or a large permeability must be present to generate such layers in natural systems. Next, the thickness of a newly formed layer is inversely related to both the buoyancy ratio and porosity, while its dependence on the thermal Rayleigh number is small.

Finally, the large velocities observed in the previous set of experiments indicate that mechanical dispersion will play a role in the transport of chemical elements. At present, the dispersivities of the geological systems studied here are poorly known but seem to depend both on the structure of the rocks and the scale of the flow domain. In order to identify the sensitivity of the layer formation to chemical dispersion, we have performed a number of experiments in which the scalar representation of the chemical dispersion is replaced by a more advanced model. In this model, chemical dispersion is related to the chemical gradient by a second order tensor, in which the velocity vector and two dispersivities appear.

From our experiments, we conclude that mechanical dispersion across the interface reduces the chemical contrast between two convective layers. Since mechanical dispersion increases the entrainment capability of the convective plumes impinging on the interface, the vertical layer scales increases as compared to the ones which develop in systems without mechanical dispersion. In case mechanical dispersion dominates the transport of solute throughout the domain, the first layer grows to the top without the formation of subsequent layers. Finally, mechanical dispersion has been taken into account in the force balance, which determines the limitation of the layer growth.

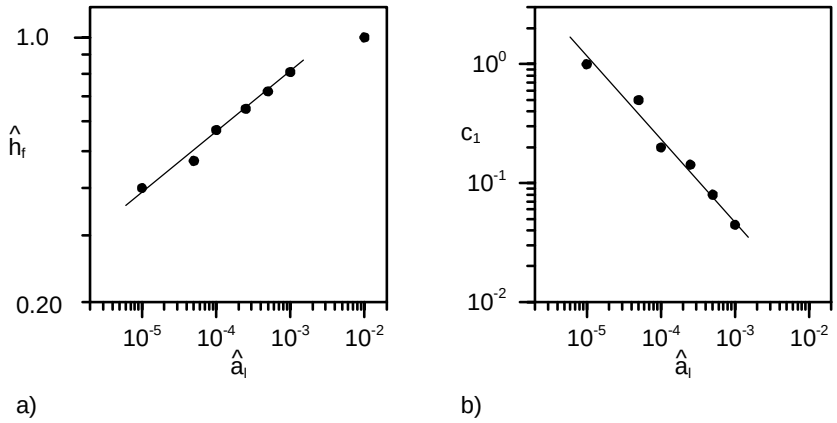

Figure 5.10: Sensitivity of behavior of the layer formation as a function the longitudinal dispersivity $\hat{a}_l$. Other parameters are $Ra_T = 10^5$, $R_\rho = 3$, $\phi^* = 0.5$, $Le_{\text{mol}} = 10^4$, and $a_r = 10$. (a) The final layer height of the first layer $\hat{h}_f$, and (b) the value which c_1 must take in order to fit the force balance (5.2).

5.4 Geophysical implications

Up to this point, we have described a mechanism by which layered structures can be generated and which also can lead to relatively sudden changes in the layer sequence. In our view, thermochemical convection in porous media offers an interesting explanation for the appearance of layered structures in intrusional bodies. The investigated scenario seems especially applicable to the mush zone at the roof of a cooling magmatic intrusion [*Marsh*, 1989]. As a first order approximation, this mush zone can be represented by a rigid matrix of connected crystals [*Kerr et al.*, 1990abc] and thus resembling a porous medium.

Within this mush zone, a stable compositional profile can develop by different mechanisms. In calc-alkaline magmas, where crystallization leaves behind a less dense melt, stable compositional profiles can develop straight away. But also in tholeiitic magmas, where the remaining melt becomes dense by crystallization, a stable compositional gradient can evolve by the *filling-box* mechanism [*Campbell*, 1996]. During formation in a slowly cooling magma chamber, the mush zone can be treated as a stagnant boundary layer of the convecting interior of the chamber. Replenishment of the intrusional body results in a heating of the compositionally stably stratified mush zone. According to our experiments, convective layers could evolve within the mush zone. Growth of the extant crystals by reaction with the interstitial liquid will then lead to the formation of chemically distinct layers. This agrees well with the observed layered structures in roof sequences of intrusion complexes (e.g., the Skaergaard or Bushveld complexes). Especially, the variety of layer scales, as found in the roof sequences [*McBirney*, 1996; *Eales and Cawthorn*, 1996], can basically result from the dynamical mechanisms which lead to sudden interface disappearance. Apart from the scenario described here, in which the driving component is heat, the experiments may also represent a situation in which both components are compositional.

On a planetary scale, thermochemical convection in porous media offers an explanation for a dynamical differentiation, rather than pure gravitational separation. During the evolution of the Earth, a situation in which a hot core is overlain by a relatively cool but still partially molten mantle is reasonable to assume [*Stevenson*, 1989]. Within the mantle itself,

gravitational differentiation could have established a stable compositional gradient thus arriving at a scenario as investigated in this chapter. Our experiments indicate that heating the mantle under such conditions from below would lead to layering of the melt, with the lowermost layer being significantly deeper than the other ones. This reflects the situation in the Earth surprisingly well, with a lower mantle being a factor of 4 deeper than the upper. As compared to layer formation in a viscous mantle (see also [*Alley and Parmentier,* 1997] for the evolution of the moon), layering in the interstitial liquid occurs on a smaller time scale.

It should be noted here, that our experiments only represent a first order approximation also for this planetary scenario, as it is assumed that the matrix is non-deformable and the fluid does not react with the solid. In a reactive magmatic body, the driving force of the interstitial liquid will be the buoyancy difference between solid and liquid [*McKenzie,* 1984], rather than the thermal forcing induced in the liquid itself as in experiments described here. The process of layer formation will also be significantly influenced by the compactive behavior of the solid material. For a study of flow in reactive deformable media, the reader is referred to [*Spiegelman et al.,* 1999].

Hydrothermal systems powered by underlying magmatic intrusions are near-surface systems which are potentially influenced by layer formation in a porous medium [*Fournier,* 1990]. From the results of laboratory experiments in a three-dimensional porous medium, *Griffiths* [1981] concluded that chemically distinct reservoirs can be maintained in hydrothermal systems. Extrapolating our results, the generation of vertically stacked layers is possible only at sufficiently large Rayleigh numbers and high buoyancy ratios. In other words, the hydrothermal system must be permeable up to considerable depths, while a large initial compositional gradient is present within the liquid. Besides these two constraints, the porosity of the rocks determines critically the stability of the layers.

Once two or more layers have developed within the hydrothermal system, the chemically distinct reservoirs can basically be maintained for a chemically dispersive time scale. During this period, which may last thousands of years, heat (solute) flux through the system is determined by the diffusion (dispersion) across the interfaces. As a consequence, the temperature in the upper fluid layer is reduced in comparison to a single-layered system [*Griffiths*, 1981]. Note, however, that interfaces could be destroyed by a dynamical mechanism at an earlier stage in the evolution of the system.

In the Salton Sea Geothermal System, California, a sharp salinity interface has been observed at a depth of 0.5 to 2.5 kilometers [*Williams*, 1997]. This interface follows the isotherm of 260°C, rather than any structural or stratigraphic feature, and separates a $NaCl, CaCl_2, KCl$ liquid with TDS (total dissolved solids) > 25 wt% from the overlying dilute fluids. These observations speak very well for a thermochemical convective system, like the one described in this study. This specific hydrothermal system was recently studied in detail by [*Oldenburg and Pruess*, 1998]. From numerical simulations, these authors concluded that thermochemical convection can explain most of the observations, though the stability of the layers depends critically on the anisotropic character of the rocks. Layering is favored only when "horizontal permeability is much larger than the vertical component". Otherwise, the convection currents penetrate the salinity interface and destroy the layering.

Provided that the force balance (equation (5.6)) is also valid in anisotropic media, this behavior can be explained in a fluid-dynamical context. In an isotropic medium, the density contrast across the salinity interface is not sufficiently strong to keep the layers separated. This leads to a breakup or migration of the interface and subsequent mixing of the two layers. By introducing a large horizontal permeability as compared to the vertical component, convection can develop within both layers while the vertical convective forces remain small. As a result, the salinity interface at depth is dynamically sustained.